Multiscale, Hierarchically Patterned Topography for Directing Human Neural Stem Cells into Functional Neurons

Kisuk Yang,[†] Hyunjung Jung,[‡] Hak-Rae Lee,[§] Jong Seung Lee,[†] Su Ran Kim,[†] Ki Yeong Song,[†] Eunji Cheong,[†] Joona Bang,[‡,*] Sung Gap Im,[§,*] and Seung-Woo Cho[†,*]

[†]Department of Biotechnology, Yonsei University, Seoul 120-749, Republic of Korea, [‡]Department of Chemical and Biological Engineering, Korea University, Seoul 136-713, Republic of Korea, and [§]Department of Chemical and Biomolecular Engineering and KI for Nanocentury, Korea Advanced Institute of Science and Technology, Daejeon 305-701, Republic of Korea

ABSTRACT Various biophysical and biochemical factors are important for determining the fate of neural stem cells (NSCs). Among biophysical signals, topographical stimulation by micro/nanopatterns has been applied to control NSC differentiation. In this study, we developed a hierarchically patterned substrate (HPS) platform that can synergistically enhance the differentiation of human NSCs (hNSCs) by simultaneously providing microscale and nanoscale spatial controls to facilitate the alignment of the cytoskeleton and the formation of focal adhesions. The multiscale HPS was fabricated by combining microgroove patterns (groove size: 1.5 μm), prepared by a conventional photolithographic process, and nanopore patterns (pore diameter: 10 nm), prepared from cylinder-forming block copolymer thin films. The hNSCs grown on the HPS exhibited not only a highly aligned, elongated morphology, but also a greatly enhanced differentiation into neuronal and astrocyte lineages, compared to hNSCs on a flat substrate (FS) or single-type patterned substrates [microgroove patterned substrate (MPS) and nanopore patterned substrate (NPS)]. Interestingly, the application of the HPS directed hNSC differentiation toward neurons rather than astrocytes. The expression of focal adhesion proteins in hNSCs was also significantly increased on the HPS compared to the FS, MPS, and NPS, likely a result of the presence of more focal contact points provided by nanopore structures. Inhibition of both β1 integrin-mediated binding and the intracellular Rho-associated protein kinase pathway of hNSCs eliminated the beneficial effects of the HPS on focal adhesion formation and actin filament alignment, which subsequently reduced hNSC differentiation. More importantly, hNSCs on the HPS differentiated into functional neurons exhibiting sodium currents and action potentials. The multiscale, hierarchically patterned topography would be useful for the design of functional biomaterial scaffolds to potentiate NSC therapeutic efficacy.

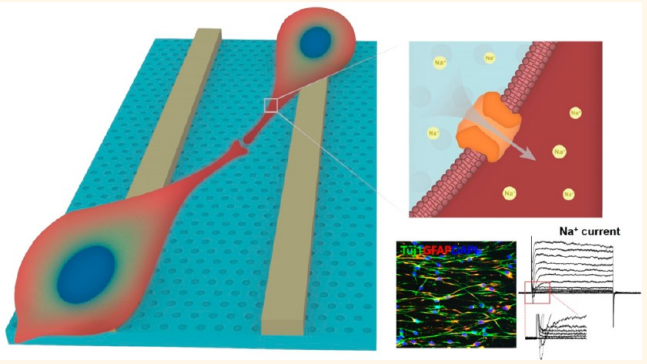

KEYWORDS: hierarchically patterned substrate · topographical stimulation · human neural stem cell · focal adhesion · cytoskeleton alignment · differentiation

The development of artificial microenvironments that achieve systematic control of stem cell fate is a key issue for effective stem cell therapies. Diverse stem cell niches regulate proliferation and differentiation of stem cells by providing biochemical signals (*e.g.*, soluble chemical factors,[1,2] growth factor proteins,[3,4] and peptides[5]), biophysical cues (*e.g.*, elastic modulus,[6−8] shear stress,[9] stiffness,[10] and geometry[11,12]), and cell−cell interactions.[13,14] In particular, the essential roles of the surface topographies of matrices and scaffolds have been highlighted to modulate adhesion, cytoskeletal organization, and differentiation of stem cells.[15−17] Indeed, stem cell differentiation can be altered by the sizes and shapes of surface topographical structures.[18−21] Our previous studies also demonstrated that substrates with a certain size of groove or pillar nanopattern significantly promote the neuronal differentiation of human neural stem cells (hNSCs) and the osteogenic differentiation of human mesenchymal stem cells (MSCs) by enhancing focal adhesion formation in these stem cells.[22,23]

* Address correspondence to joona@korea.ac.kr, sgim@kaist.ac.kr, seungwoocho@yonsei.ac.kr.

Received for review February 28, 2014 and accepted July 22, 2014.

Published online July 22, 2014
10.1021/nn501182f

© 2014 American Chemical Society

Substrates containing the hierarchical structures of microscale and nanoscale patterns allow for more efficient spatial control of stem cell differentiation *via* the simultaneous modulation of the alignment of the cytoskeleton and intracellular focal adhesion protein assembly. Patterned topographies with cell dimensions ranging from submicrometers to tens of micrometers directly influence the alignment and orientation of stem cells by inducing cellular morphological changes along the patterns. This process leads to the rearrangement of the cytoskeleton, alterations of the shape of the nucleus, and changes in the expression levels of genes involved in stem cell differentiation.[24] Nanometer-sized patterns with the dimensions of integrin (8−12 nm),[25,26] important transmembrane receptor proteins involved in signal transduction from extracellular matrices (ECMs) to cells, induce nanoscale integrin clustering, which activates the integrin-mediated intracellular signaling cascade for stem cell differentiation.[27] However, there are few studies reporting spatial control of stem cell differentiation using patterned topographies with different spatial dimensions ranging from nanometers to micrometers as a result of difficulties in the fabrication of such multiscale, hierarchically patterned structures on a single substrate.[28] To generate functional substrates for the spatial control of stem cell adhesion, alignment, and differentiation, it is essential to fabricate hierarchical patterns that incorporate a few tens of nanometer-sized patterns into microscale structures in a reliable, reproducible way, which remains challenging.

Among several possible approaches for such nanofabrication, the self-assembly of block copolymer (BCP) can be applied to produce such hierarchical patterns. The self-assembly of BCP has been used as an attractive strategy for fabricating uniform nanopatterns over large areas.[29] This method can produce various nanoscopic structures, including spheres, cylinders, bicontinuous gyroids, and lamellae, depending on the block composition and chain architecture of the BCPs. The feature sizes of the microdomains prepared by BCP self-assembly range from approximately 5 to 50 nm, which match well with those of relevant proteins (*e.g.*, integrins), but it is quite difficult to obtain this range of patterns by conventional photolithography processes.[29−31] However, such microdomain sizes are relatively easy to achieve using the BCP method, and the control of pattern size is systematically tunable by simply varying the molecular weights of the BCPs. From a practical point of view, the nanopatterns from BCPs can be fabricated over large areas (>150 × 150 mm^2) using a simple spin-casting process;[32] thus, it is an inexpensive process compared to other conventional lithographic techniques to access sub-50 nm resolution. Moreover, it has been confirmed that the mechanical properties of BCP films are comparable to those of conventional photoresists, and thus the BCP process is quite compatible with current photolithographic conditions for the fabrication of microgroove-patterned structures.[30]

In this study, we developed substrates with well-defined hierarchically patterned topographies through a bottom-up assembly of microscale groove patterns and nanometer-scale pore structures. Large-area hierarchical patterns were fabricated using a combination of selective etching of phase-segregated BCPs and standard photolithography. Using this process, a hierarchical pattern with nanopores (10 nm diameter) incorporated into the microgroove structures (1.5-μm width) was prepared on a large surface of 25 × 25 mm^2. The hNSCs grown on these hierarchical patterns exhibited significantly enhanced focal adhesion development, aligned cytoskeletal morphogenesis, and neuronal differentiation compared to hNSCs on a flat silicon substrate or single-type patterned substrate due to the integrated spatial control of actin filament alignment along the microgroove structures and focal adhesion formation by nanopores. More importantly, the hierarchical patterns directed hNSCs into electrophysiologically active neurons exhibiting sodium currents and action potentials. To the best of our knowledge, this is the first study reporting the generation of functional neurons from hNSCs using the patterned substrates. Our study suggests the effective use of hierarchically patterned topography for the delicate regulation of stem cell differentiation.

RESULTS AND DISCUSSION

Fabrication of Hierarchically Patterned Substrate (HPS). In this study, four types of substrates were prepared: flat substrate (FS), nanopore patterned substrate (NPS) from BCPs, microgroove patterned substrate (MPS), and hierarchically patterned substrate (HPS) consisting of both microgroove and nanopore patterns (Figure 1). For the preparation of HPS, microgroove structures incorporated with BCP nanopore patterns were formed *via* a conventional photolithography technique. In this case, it is critical that the underlying BCP films are cross-linked to avoid perturbations from various organic solvents used during the photolithography process,[32−35] which is extremely challenging and expensive in other lithography techniques such as E-beam lithography. For this purpose, we synthesized a cross-linkable BCP poly(styrene-*b*-methyl methacrylate) (PS-*b*-PMMA), *via* reversible-addition−fragmentation chain transfer (RAFT) polymerization containing Meldrum's acid in a styrene block (Supporting Information, Figure S1). Meldrum's acid can generate reactive ketene functional groups upon heating, allowing for cross-linking *via* dimerization.[33,34] The total molecular weight of cross-linkable PS-*b*-PMMA was controlled to 61 000 g/mol with 32% (v/v) of PMMA block; thus, it exhibits a cylindrical microstructure.

For the preparation of NPS, a solution of cross-linkable PS-*b*-PMMA was spin-cast on a silicon wafer

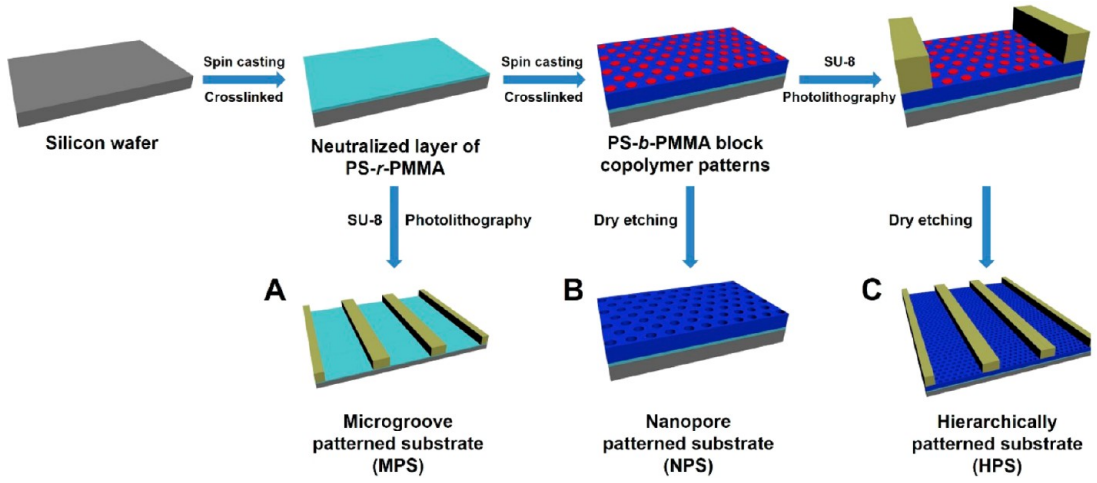

Figure 1. Schematic illustration of the fabrication of various topographic-patterned substrates. (A) Microgroove-patterned substrate (MPS), (B) nanopore-patterned substrate (NPS), and (C) hierarchically patterned substrate (HPS).

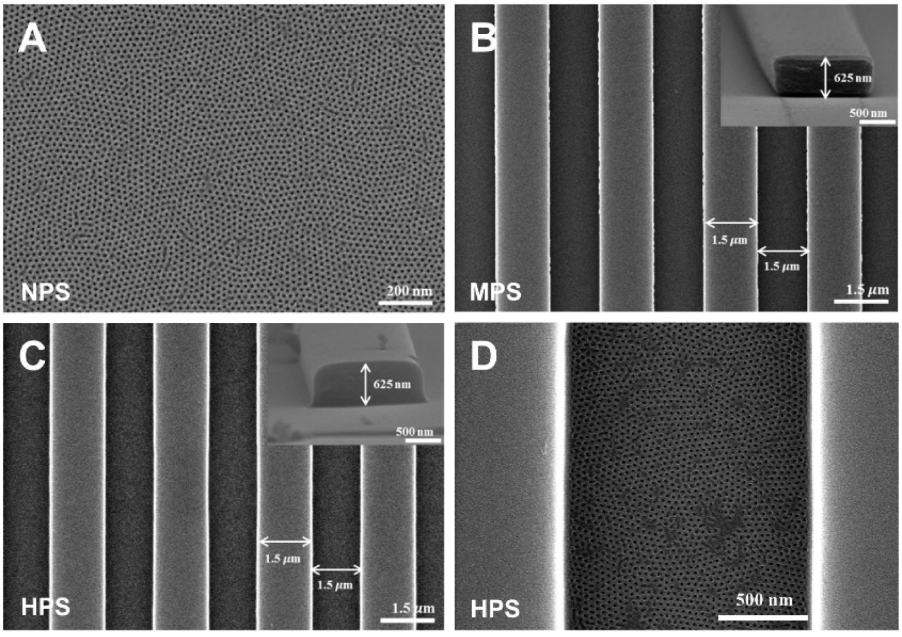

Figure 2. SEM images of (A) BCP nanopore patterns, (B) microgroove patterns, and (C) hierarchical patterns. (D) High magnification image of hierarchical patterns shown in (C).

neutralized with PS-*r*-PMMA random copolymers (Figure 1). Film thickness was controlled to be approximately 35 nm, and the films were thermally annealed at 190 °C for 48 h, leading to perpendicularly oriented cylindrical patterns. To generate nanopore patterns, the PMMA block was selectively removed by reactive ion etching (Figure 1B). The domain spacing and pore sizes of the nanopatterns were 28 and 10 nm, respectively (Figure 2A). The micrometer-sized groove patterns were prepared by standard I-line photolithography with an SU-8 photoresist (Figure 1A). For the fabrication of the hierarchical patterns, the PS-*b*-PMMA thin films were first prepared by the aforementioned procedure, and then the films were thermally cross-linked at 250 °C for 10 min under nitrogen. After fabricating the microgroove patterns *via* standard photolithography with an SU-8 photoresist, the PMMA domains were removed by reactive ion etching (Figure 1C). As seen in Figure 2D, the nanopore patterns were formed between the groove trenches, indicating that the BCP films were efficiently cross-linked and the resulting nanopatterns were not affected by the photolithography process. In both the microgroove and hierarchical patterns, the distance between the groove patterns was 1.5 μm (Figure 2B,C).

Enhancement of Cytoskeletal Alignment and Focal Adhesion Formation of hNSCs by Hierarchical Patterns. The application of hierarchical patterns facilitated cytoskeletal alignment of hNSCs and significantly promoted focal adhesion development of hNSCs. Phalloidin staining of the

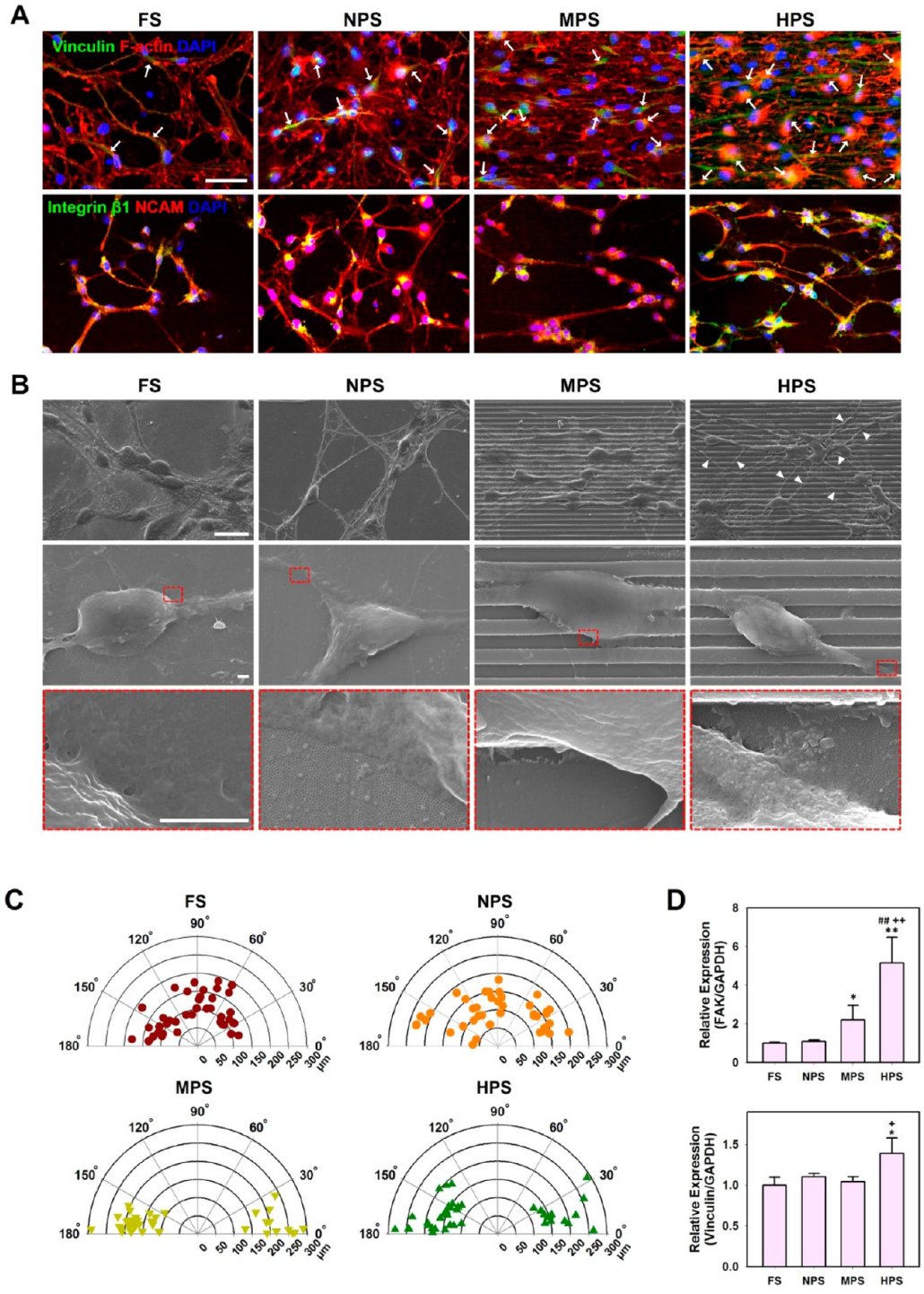

Figure 3. Focal adhesion and alignment of the cytoskeleton of hNSCs on the substrates after 5 days in culture. (A) Staining of the cytoskeleton (F-actin; red) and focal adhesion protein vinculin (yellow/green) in hNSCs on the FS, NPS, MPS, and HPS; scale bar = 50 μm. The white arrows indicate the focal adhesion points. Co-localization of the adhesion molecule (NCAM) and integrin β1 (yellow) in hNSCs on the FS, NPS, MPS, and HPS. (B) SEM images of hNSCs on each substrate; scale bar = 20 μm. The white arrowheads indicate sprouting of neurites from cell bodies across the microgroove patterns (top rows). High magnification images of hNSCs on each substrate (middle and bottom rows); scale bars = 1 μm. (C) Orientation of hNSCs grown on each substrate (n = 40) represented in the compass plots. (D) qRT-PCR analysis to examine the expression of focal adhesion protein genes (FAK and vinculin) in hNSCs grown on each substrate (n = 3; *p < 0.05, **p < 0.01, compared to the FS group; $^{\#\#}p$ < 0.01, compared to the NPS group; ^{+}p < 0.05, ^{++}p < 0.01, compared to the MPS group).

cytoskeleton (filamentous actin; F-actin) showed that hNSCs cultured on the MPS and HPS exhibited the highly elongated alignment of actin filaments along the patterned groove (Figure 3A). In contrast, hNSCs on either the FS or NPS did not show such an extended, actin-aligned morphology (Figure 3A). The immunofluorescent

staining for vinculin, a representative focal adhesion protein, indicated that focal adhesion formation of hNSCs was significantly enhanced on the HPS compared to other control substrates (FS, NPS, and MPS) (Figure 3A; arrows), possibly as the result of the presence of more focal contact points provided by nanopore structures incorporated into the HPS. The colocalization of integrin β1 and neural cell adhesion molecule (NCAM) was significantly enhanced in the hNSCs grown on the HPS compared to the cells on other control substrates (FS, NPS, and MPS) (Figure 3A; yellow), indicating a significant enhancement of focal adhesion development in the hNSCs by hierarchically patterned topography. Given that the size of integrin is 8−12 nm,[25] the nanopore structures of 10 nm diameter on the HPS may serve as focal adhesion contact points that are capable of interacting with single integrin molecules.

Scanning electron microscopy (SEM) also revealed an extended, aligned cellular morphology of hNSCs along the microgroove patterns on the MPS and HPS (Figure 3B). Interestingly, it appears that HPS increases the sprouting of neurites from cell bodies across the microgroove patterns (Figure 3B, top rows; arrowheads), which was less observed on the MPS (Figure 3B, top rows). This finding may also be attributed to nanopore structures that provide potential contact points for focal adhesion. Neurite sprouting across the cells can enhance cell−cell interactions by increasing direct contact with neighboring cells. HPS induced the direct and simultaneous contact of hNSCs with both types of surface topographies of microgroove and nanopore patterns (Figure 3B, middle and bottom rows). This data indicates that HPS can provide synergistic topographical stimulation to promote focal adhesion formation and subsequent differentiation of hNSCs. Most of the differentiated hNSCs on the MPS and HPS were oriented along the microgroove patterns, whereas hNSCs on either the FS or NPS exhibited random orientations (Figure 3C). Quantitative real-time polymerase chain reaction (qRT-PCR) revealed that the expression of genes for focal adhesion kinase (FAK) and vinculin in the hNSCs was significantly increased ($p < 0.05$) on the HPS compared to other control substrates (FS, NPS, and MPS) (Figure 3D), indicating the enhanced focal adhesion formation in the hNSCs on the HPS.

To confirm that nanopore topography is essential for enhancing focal adhesion development, we investigated whether the coating of ECMs that can bind to integrin β1 on the hNSCs can replace the nanopore structures of the HPS. Since laminin is one of the major ECM types that bind to integrin β1 and has been widely used for neuron and NSC culture,[4] the relative gene expression of focal adhesion proteins (vinculin and FAK) was compared between the hNSCs cultured on the MPS coated with laminin proteins and the hNSCs cultured on other substrates (Supporting Information, Figure S2). qRT-PCR analysis showed that laminin coating on the MPS did not increase significantly the mRNA expression of vinculin and FAK in the hNSCs (Supporting Information, Figure S2; MPS *versus* MPS-LM). The gene expression level of vinculin and FAK was lower in the hNSCs cultured on the MPS coated with laminin proteins than in the hNSCs cultured on the HPS (Supporting Information, Figure S2; HPS *versus* MPS-LM). These results indicate that the nanopore structures (10 nm diameter) in the hierarchically patterned topography cannot be replaced by a simple ECM coating and are indispensable for focal adhesion formation enhancement.

Enhanced Differentiation of hNSCs by Hierarchical Patterns. The promotion of F-actin alignment and focal adhesion formation of hNSCs on the HPS can lead to significant enhancement of hNSC differentiation. Activation of the FAK pathway following cytoskeletal rearrangement and focal adhesion formation is known to stimulate downstream signals for stem cell differentiation.[22,36] Moreover, an increase in cell−cell contact by hierarchical patterns may be able to further enhance hNSC differentiation *via* the stimulation of cell−cell signaling.[37] Therefore, we hypothesized that the hierarchical patterns containing both microgroove and nanopore structures can generate synergistic effects on the enhancement of hNSC differentiation by improving cytoskeletal reorganization, FAK pathway activation, and cell−cell interactions, which are early events in mechanotransduction signal pathways involved in stem cell differentiation. To test this hypothesis, we cultured hNSCs on each substrate under spontaneous differentiation medium conditions without supplementation of mitogenic growth factors such as basic fibroblast growth factor (bFGF) and leukemia inhibitory factor (LIF).

The combination of microgroove structures and nanopore patterns constructed on the HPS significantly enhanced the differentiation of hNSCs compared with the FS or single-type patterned substrates (MPS and NPS). Immunocytochemical staining for neuronal markers [neuronal class III β-tubulin (Tuj1) and microtubule-associated protein 2 (MAP2)] and astrocyte marker [glial fibrillary acidic protein (GFAP)] revealed the alignment of Tuj1-positive neurites, MAP2-positive cell bodies, and GFAP-positive intermediate filaments along the microgroove patterns on the MPS and HPS (Figure 4A). Neurite formation was the most extensive in the HPS group compared to other control substrate groups (Figure 4B). The hNSCs differentiated on the HPS exhibited much longer neurite outgrowth than the cells on the control substrates (Figure 4B). These data indicate that neurite formation and outgrowth of hNSCs during differentiation were enhanced by hierarchically patterned topography.

A qRT-PCR analysis revealed that the expression of genes for neuronal markers (Tuj1 and MAP2) and an

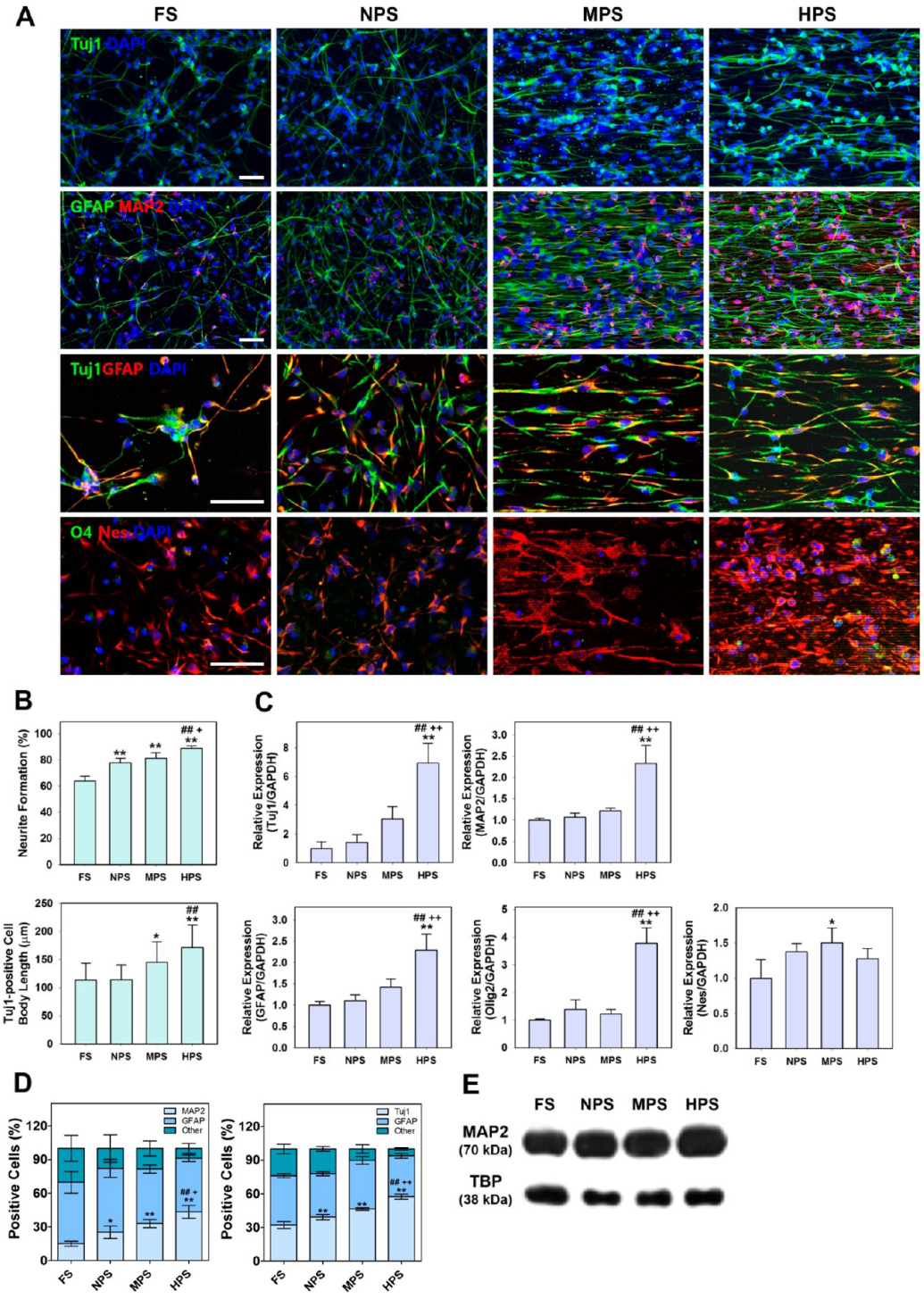

Figure 4. Differentiation of hNSCs on the substrates after 5 days in culture. (A) Immunofluorescent staining of hNSCs differentiated on each substrate for neuronal (Tuj1 and MAP2), astrocyte (GFAP), oligodendrocyte (O4), and undifferentiated NSC (nestin) markers; scale bars = 50 μm. (B) Quantification of neurite formation ($n = 4$) and the length of neurite outgrowth ($n = 15$) in the Tuj1-stained images (*$p < 0.05$, **$p < 0.01$, compared to the FS group; $^{\#\#}p < 0.01$, compared to the NPS group; $^{+}p < 0.05$, compared to the MPS group). (C) qRT-PCR analysis to measure the expression of the genes for Tuj1, MAP2, GFAP, Olig2, and nestin in hNSCs grown on each substrate ($n = 3$; *$p < 0.05$, **$p < 0.01$, compared to the FS group; $^{\#\#}p < 0.01$, compared to the NPS group; $^{++}p < 0.01$, compared to the MPS group). (D) Relative proportion of MAP2- or GFAP-positive cells and Tuj1- or GFAP-positive cells on each substrate ($n = 4$; *$p < 0.05$, **$p < 0.01$, compared to the FS group; $^{\#\#}p < 0.01$, compared to the NPS group; $^{+}p < 0.05$, $^{++}p < 0.01$, compared to the MPS group). (E) Western blot analysis of MAP2 protein expression in hNSCs grown on each substrate. A nuclear protein (TATA binding protein; TBP) was used as a loading control for the comparison of MAP2 protein expression.

astrocyte marker (GFAP) was significantly upregulated in hNSCs grown on the HPS compared to hNSCs grown on the FS, MPS, and NPS (Figure 4C), indicating enhanced differentiation of hNSCs into neuron and

astrocyte lineage by hierarchical patterns. Immunofluorescent staining and qRT-PCR analysis for examining the expression of other cell phenotype markers (oligodendrocyte lineage markers; O4 and oligodendrocyte transcription factor 2 (Olig2) and undifferentiated NSC marker; nestin) (Figure 4A,C) showed that the expression of O4 and Olig2 was significantly increased in the hNSCs grown on the HPS compared to the cells on other control substrates (FS, NPS, and MPS) (Figure 4A,C). The gene expression of nestin was not significantly different between the groups (Figure 4C). These results imply that HPS promotes hNSC differentiation including oligodendrocyte lineage as well as neuron and astrocyte and does not affect self-renewal and undifferentiated status of hNSCs. Together our results demonstrate that hierarchically patterned topography can accelerate hNSC differentiation but does not support self-renewal of hNSCs.

More interestingly, the population of MAP2-positive neuronal lineage cells was increased on the HPS (43.5 $\pm$ 5.7% *vs* FS 15.1 $\pm$ 2.3%, NPS 25.4 $\pm$ 5.6%, and MPS 33.0 $\pm$ 3.7%), whereas the relative population of GFAP-positive astrocytes was concurrently decreased on the HPS (47.7 $\pm$ 3.1% *vs* FS 54.6 $\pm$ 9.6%, NPS 56.8 $\pm$ 8.0%, and MPS 48.6% $\pm$ 3.6%) (Figure 4D), suggesting that hierarchical patterns direct the fate of differentiated hNSCs to a neuronal lineage rather than a glial lineage. The proportion of Tuj1-positive cells relative to GFAP-positive cells was also increased on the HPS compared to other substrates (FS, NPS, and MPS), confirming the promoted differentiation of hNSCs toward a neuronal lineage on the HPS (Figure 4D). Western blot analysis to compare the relative expression of MAP2 protein in the hNSCs grown on each substrate indicated that MAP2 protein expression was enhanced by hierarchically patterned topography (Figure 4E).

In this study, NPS alone did not enhance the gene expression of focal adhesion proteins including FAK and vinculin (Figure 3D). We think that pore patterns may be relatively less effective in focal adhesion development than pillar and groove patterns with the protruded structures. Although the nanopore pattern alone did not promote focal adhesion development, it could synergistically enhance focal adhesion formation in the hNSCs when incorporated into MPS (Figure 3D), ultimately leading to enhanced neuronal differentiation of hNSCs on the HPS (Figure 4C,D). This indicates that spatial distribution of surface topographies as well as topography shapes and dimensions is also critical for focal adhesion formation and differentiation of stem cells. Therefore, our results suggest that hierarchically patterned topographies capable of facilitating focal adhesion formation are required for the development of biomaterial scaffolds promoting stem cell differentiation or lineage specification of stem cells.

Mechanotransduction Mechanism of Enhanced Differentiation of hNSCs by Hierarchical Patterns. Topographical stimulation by hierarchical patterns may enhance hNSC differentiation by activating intracellular mechanotransduction pathways initiated from integrin-mediated binding to substrates. The cell-matrix interaction *via* integrin binding is important for the regulation of various cellular behaviors, such as adhesion, spreading, proliferation, and differentiation.[38] Integrin activation induced by specific nanotopographical features can promote focal adhesion development and activate the FAK pathway,[36] which ultimately induces stem cell differentiation.[17,36,39] Thus, the HPS with nanopore structures of integrin dimensions (10 nm) may enable integrin-mediated activation of the FAK pathway for enhanced hNSC differentiation by facilitating integrin binding of hNSCs onto the nanopores.

Rho-associated protein kinase (ROCK), one of the key regulators of cytoskeletal organization, can also serve as a transducer of mechanical signals from hierarchical patterns.[40] Considering that ROCK modulates mechanotransduction pathways affecting stem cell differentiation, such as focal adhesion formation, actin organization, and FAK phosphorylation,[40] ROCK might be a potential modulator of hNSC differentiation and lineage specification promoted by hierarchical patterns. Several studies have indeed reported that substrates with a specific topography, pattern shape, and stiffness accelerate osteogenic differentiation of MSCs *via* focal adhesion and actin polymerization enhanced by the ROCK signaling pathway.[12,41,42]

Inhibition studies using integrin antibodies and an inhibitor of the ROCK pathway performed in our study confirmed that a series of mechanotransduction events, including integrin binding, F-actin reorganization, and focal adhesion assembly, are involved in enhanced differentiation of hNSCs by the hierarchically patterned topography (Figure 5). In our study, all tested substrates were coated with fibronectin to facilitate hNSC adhesion and antibodies against β1 integrin, which binds to fibronectin, were used to block hNSC adhesion onto the fibronectin-coated substrates. Addition of β1-integrin antibodies disrupted adhesion and alignment of hNSCs along the patterns, which eliminated the effects of the hierarchical patterns on the focal adhesion formation (Figure 5A) and the enhanced differentiation of hNSCs into neurons and astrocytes (Figure 5B). Treatment with Y27632, a ROCK inhibitor, also interrupted hNSC alignment (Figure 5A) and reduced differentiation of hNSCs (Figure 5B). qRT-PCR analysis of focal adhesion proteins (FAK and vinculin) indicated that gene expression of FAK and vinculin in the hNSCs on each substrate was reduced by treatment with both β1-integrin antibodies and Y27632 compared to no treatment (Figure 5C). In particular, a reduction in gene expression was most significant in hNSCs cultured on the HPS compared to hNSCs cultured on other control substrates (FS, NPS, and MPS) (Figure 5C). Accordingly, the expression levels of differentiation marker genes (neuron: Tuj1; astrocyte: GFAP) enhanced by the hierarchical

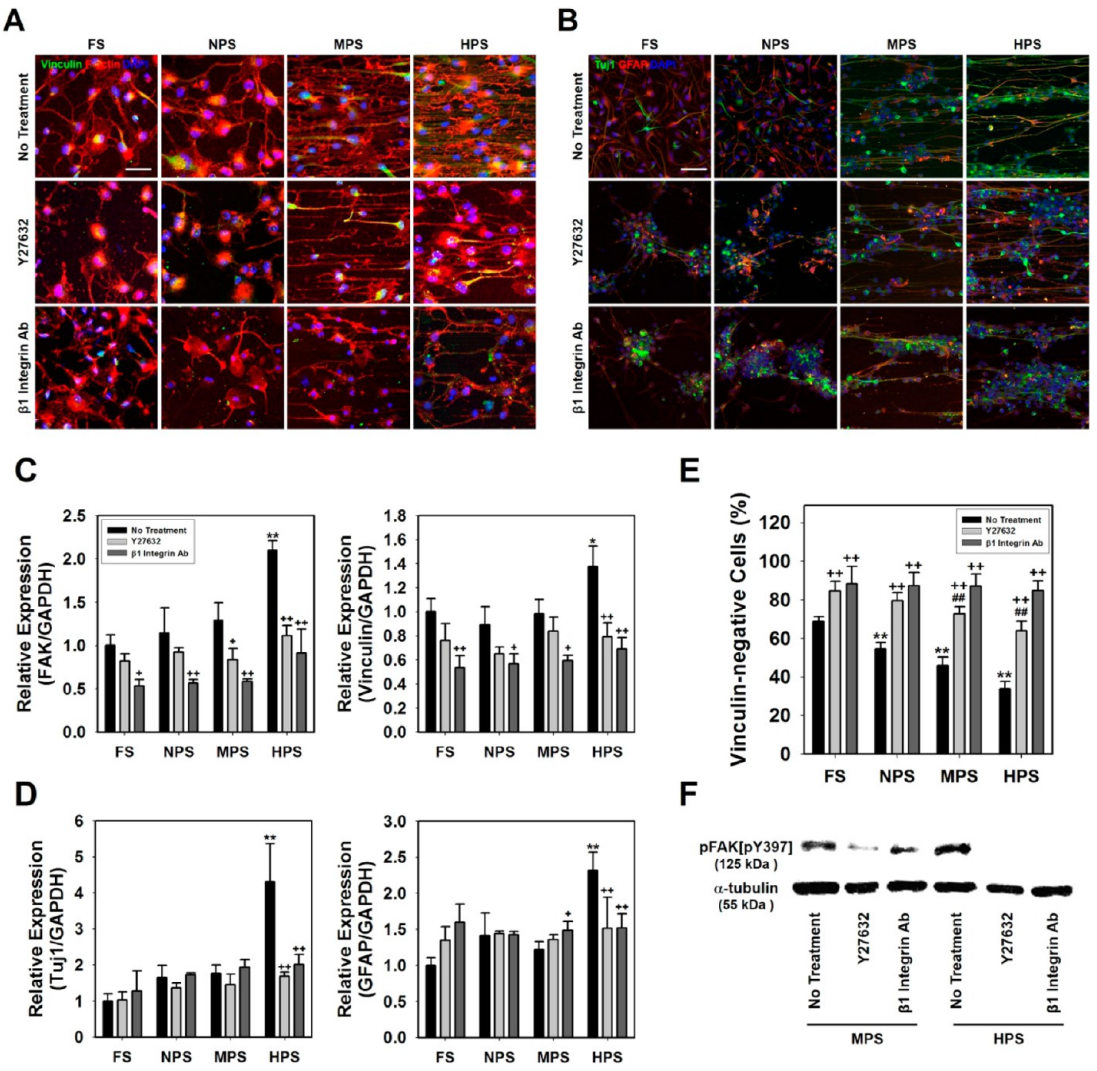

Figure 5. Inhibition of focal adhesion, alignment of the cytoskeleton, and differentiation of hNSCs by treatments with the ROCK inhibitor (Y27632) and β1-integrin antibodies (after 1 day in culture). (A) Staining of focal adhesion protein (vinculin) and cytoskeleton (F-actin) and (B) immunofluorescent Tuj1 and GFAP staining of hNSCs on each substrate with or without treatment with Y27632 and β1-integrin antibodies; scale bars = 50 μm. Cell nuclei were counterstained with DAPI. qRT-PCR was performed to examine the expression of genes for (C) focal adhesion proteins (FAK and vinculin) and (D) differentiation markers (Tuj1 and GFAP) in hNSCs on each substrate with or without treatment with Y27632 and β1-integrin antibodies (*p < 0.05, **p < 0.01 *versus* the untreated FS group; ^{+}p < 0.05, ^{++}p < 0.01 *versus* the no-treatment group of each substrate). (E) Quantification of nonadherent cells (vinculin-negative cells) in the vinculin- and F-actin-stained images (n = 4; **p < 0.01 *versus* the untreated FS group; $^{\#\#}p$ < 0.01 *versus* the Y27632-treated FS group; ^{++}p < 0.01 *versus* the no-treatment group of each substrate). (F) Western blot to compare the expression of phosphorylated FAK [pFAK(Y397)] in hNSCs cultured on the MPS and HPS with or without treatment with Y27632 and β1-integrin antibodies.

patterns were significantly decreased by treatment with β1-integrin antibodies and Y27632 (Figure 5D).

The level of nonadherent cells defined as vinculin-negative cells was quantified on each substrate 1 day after treatments of integrin β1 antibodies and Y27632 (Figure 5E). In case of hNSCs without treatments of integrin β1 antibodies and Y27632 (no treatment), the proportion of nonadherent cells was the lowest in the HPS group compared to other substrate groups (FS, NPS, and MPS) (Figure 5E). The treatments of integrin β1 antibodies and Y27632 significantly increased the level of nonadherent cells on all substrates (Figure 5E), indicating that integrin β1-mediated binding and ROCK pathway are critical for focal adhesion of hNSCs on the patterned substrates. Western blot analysis revealed that phosphorylation of FAK was enhanced in hNSCs on the HPS compared to the cells on the MPS, indicating the activation of the FAK pathway by the hierarchical patterns (Figure 5F). Treatment with both β1-integrin antibodies and Y27632 significantly reduced FAK phosphorylation in hNSCs grown on the HPS (Figure 5F). Overall, these data demonstrate that β1 integrin-mediated binding and ROCK-mediated intracellular signaling pathways are responsible for the promotion of focal adhesion formation, FAK pathway activation, and, in turn, the enhanced differentiation of

hNSCs on the HPS, which may suggest potential mechanotransduction mechanisms of hNSC differentiation enhanced by hierarchical patterns.

The viability of hNSCs treated with integrin β1 antibodies and ROCK inhibitor (Y27632) was examined because integrin binding and ROCK pathway are known to be involved in various cellular functions including survival and proliferation in addition to adhesion.[17,36] Live/Dead staining and 3-(4,5-dimethylthiazol-2-yl)-2,5-diphenyltetrazolium bromide (MTT) assay of the hNSCs treated with integrin β1 antibodies and Y27632 (Supporting Information, Figure S3) indicated that these treatments disrupted alignment and elongation of hNSCs along the patterns but did not reduce the viability and mitochondrial metabolic activity of hNSCs on each substrate. The treated hNSCs did not exhibit strong adhesion and extended cellular morphology, but most cells were viable 1 day after the treatments (Supporting Information, Figure S3A). MTT assay of hNSCs treated with integrin β1 antibodies and Y27632 also indicated that the treated cells showed similar mitochondrial metabolic activity and proliferative ability to nontreated cells (Supporting Information, Figure S3B). In our study, these treatments decreased adhesion, alignment, and elongation of hNSCs on the patterned surface topographies, but did not reduce the viability, survival, and metabolic activity of hNSCs on each substrate due probably to the optimized doses of each treatment that do not affect the cell survival while diminishing the effect of substrate topographies.[17,36]

The strategy of modulating cytoskeleton organization can be considered to further enhance neuronal differentiation of stem cells. Several recent studies report the matrix stiffness- and rigidity-dependent manipulation of stem cell differentiation *via* mechanotransduction signaling pathways.[10,43−45] Modulation of actomyosin cytoskeleton integrity, contractility, and organization in stem cells by matrix stiffness and rigidity was found to regulate mechanosensitive transcription factor activity and ultimately alter stem cell differentiation.[10,43−45] Although we did not examine the effects of the stiffness and rigidity of patterned substrates on focal adhesion formation and differentiation of hNSCs, it would be an interesting future study to employ a substrate-induced modulation of cytoskeleton integrity and organization for activating mechanotransduction signal pathways, which can render stem cells more sensitive to geometry features and ultimately enhance stem cell differentiation.

In this study, we used α-tubulin as a loading control for Western blot analysis to check FAK phosphorylation (Figure 5F). Glyceraldehyde 3-phosphate dehydrogenase (GAPDH) was applied as a housekeeping control for normalization of target gene expression in qRT-PCR analysis (Figures 3D, 4C, 5C,D). α-tubulin is a cytoskeletal microtubule protein and GAPDH is recently found to be implicated in axonal transport.[46] Thus, the expression of these molecules (α-tubulin and GAPDH) may be altered by microtubule dynamics and axonal reorganization. These molecules have been typically applied as the standard controls for Western blot and qRT-PCR analysis, but they may not be the most appropriate controls for our study because the expression of these molecules might be affected by cytoskeletal and microtubule dynamics altered by substrate topographies. Therefore, it would be more appropriate to use other loading or normalization control less affected by microtubule dynamics such as nuclear proteins. For these reasons, a nuclear protein (TATA binding protein; TBP) was tested as a loading control in Western blot analysis for the comparison of MAP2 protein expression (Figure 4E).

Functional Neuronal Differentiation of hNSCs on the Hierarchically Patterned Substrate (HPS). We examined whether neurons differentiated from hNSCs on the HPS are electrophysiologically active. Whole cell patch clamp was performed to determine the electrophysiological properties of the cells 5 days after hNSC culture on the HPS as previous studies reported that Na^+ currents and action potentials are observed when hNSCs differentiate to neurons.[47,48] In the voltage clamp mode, voltage-activated currents were recorded from the hNSC-differentiated neurons (Figure 6A). Membrane potential was hold to −60 mV and sequential voltage steps with 10 mV steps were given ranged from −50 to +50 mV. A transient inward current was followed by slower outward current responding to voltage steps. The transient inward current generally represents the voltage activated Na^+ current and the outward current with slower kinetics represents the K^+ currents. We could not observe the transient inward current in nondifferentiated hNSCs (data not shown), indicating that this inward current appears only when hNSCs differentiated to neurons. The maximum peak amplitude of transient inward current was −120.8 pA.

Next, we injected depolarized currents into the cells to depolarize the membrane potential in the current clamp mode. The action potential was generated only in the cells which showed inward currents (Figure 6B), suggesting that the channel mediating transient inward currents also produces action potential. To identify that the channels which mediated currents and spikes were voltage-activated Na^+ channels, Na^+ channel antagonist tetrodotoxin (TTX) was applied in the bath for 5−10 min. TTX blocked Na^+ channels, and action potentials and Na^+ currents were completely disappeared (Figure 6A,B, after TTX) showing that the currents and spikes in previous recording were mediated by Na^+ channel. Together these results suggest that some of hNSCs cultured on the HPS could differentiate into functional neurons that are excitable and can respond to electrical stimuli. To the best of our knowledge, this is the first study reporting the generation of electrophysiologically active, functional neurons from hNSCs on the patterned substrates.

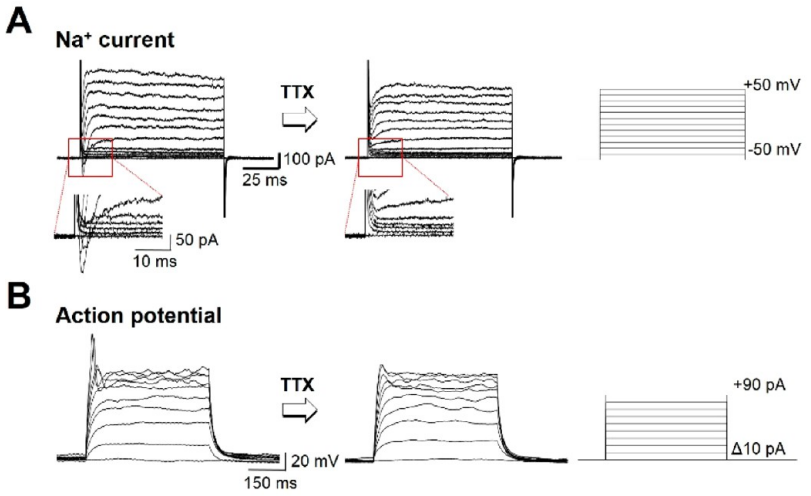

Figure 6. Whole-cell patch clamping to detect Na^+ channel-mediated currents and action potential spikes generated in differentiated hNSCs on the HPS. (A) Recording of Na^+ currents in the neurons differentiated from hNSCs on the HPS. Electrical stimulations from −60 to +50 mV (right) were applied into the patched cells, and transient inward currents were recorded (left). These currents were abolished after treatment of 0.5 μM TTX (Na^+ channel blocker) (middle), suggesting that these currents were mediated by Na^+ channels. Enlarged traces (in red boxes) reveal the presence of transient inward currents (before TTX treatment) and their disappearance (after TTX treatment) more clearly. (B) Action potential spikes were generated in response to the depolarizing current injections (left). These action potential spikes were also blocked by TTX treatment (middle).

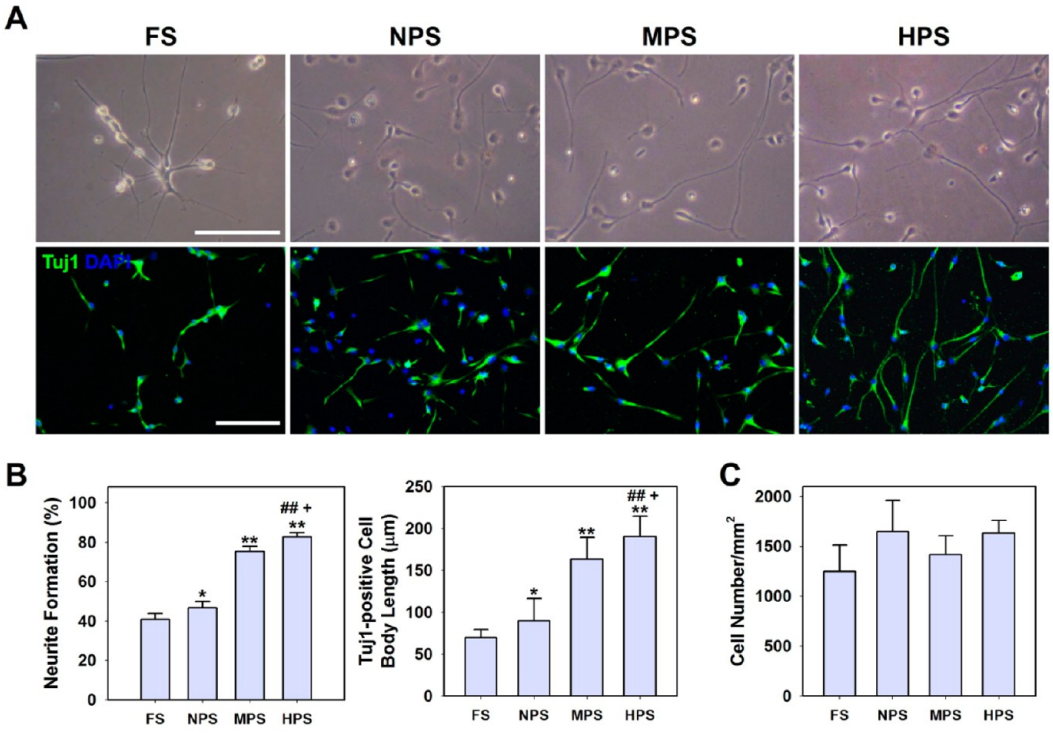

Figure 7. Maintenance of functional neuronal phenotype of hNSCs harvested from the HPS. (A) Light microscopic observation and immunofluorescent neuronal marker (Tuj1) staining of hNSCs cultured on the tissue culture polystyrene plate for 4 days; scale bars = 50 μm. The hNSCs were harvested from patterned substrates and transferred onto the flat tissue culture polystyrene plate. (B) The level of neurite formation ($n = 4$) and the length of neurite outgrowth ($n = 11$) quantified from Tuj1-stained images (*$p < 0.05$, **$p < 0.01$, compared to the FS group; $^{\#\#}p < 0.01$, compared to the NPS group; $^{+}p < 0.05$, compared to the MPS group). (C) The density of hNSCs cultured on the tissue culture polystyrene plate for 4 days after cell transfer.

Mechanical Memory of hNSCs Harvested from the Hierarchically Patterned Substrate (HPS) to Maintain Their Functional Neuronal Phenotype. Finally, we examined whether the hNSCs exhibiting enhanced neuronal differentiation on the HPS can still maintain such phenotypes after being harvested from the HPS. Interestingly, microscopic observation and neuronal marker staining (Tuj1) indicated that hNSCs harvested from the HPS and

transferred onto the flat polystyrene culture plate exhibit cellular morphology with highly extended, elongated neurites even after the hierarchically patterned topographies are removed (Figure 7A). The level of neurite formation and the length of neurite outgrowth were much greater in the hNSCs harvested from the HPS than in the cells from other control substrates (FS, NPS, and MPS) (Figure 7B). The cell density was not significantly different between the groups (Figure 7C). This data, together with Figure 7A, B, indicates that the attachment and growth levels of hNSCs harvested from the HPS were similar to hNSCs from other control substrates, but only hNSCs from the HPS exhibited enhanced neuronal differentiation even after being transferred onto new culture substrates. These results suggest that hNSCs harvested from the HPS retain the capability of enhanced neuronal differentiation and functional neuronal phenotypes, which may be implicated in a mechanical memory of stem cells; stem cells remember the information from past mechanical and physical environments.[44] This is important in that mechanical memory of stem cells can influence a long-term fate of stem cells even after transplantation into the body.[44] Therefore, HPS can provide an efficient stem cell culture platform to produce functional neuronal lineage cells possessing the improved regenerative potential for neural tissue engineering or neurodegenerative disease treatment.

CONCLUSIONS

In summary, the multiscale, hierarchical patterned topographies of microgroove and nanopore structures enhanced focal adhesion formation and differentiation of hNSCs. The BCP nanopore-patterned topography that mimics the dimension of integrin molecules could be incorporated into the microgroove-patterned structures in a simple, reproducible, and cost-effective manner. The fabricated HPS not only promoted hNSC differentiation, but also directed hNSC lineage specification into functional neurons exhibiting sodium currents and action potentials. The enhanced neuronal differentiation of hNSCs on the HPS appears to be associated with a series of mechanotransduction events, such as integrin binding, focal adhesion formation, alignment of the cytoskeleton, FAK activation, and stimulation of the ROCK pathway. The hierarchical patterning technique to incorporate multiple scales and diverse pattern shapes would be useful for the development of functional biomaterial scaffolds with surface topographies to potentiate the therapeutic efficacy of stem cells.

MATERIALS AND METHODS

Synthesis of Cross-Linkable BCP. Thermally cross-linkable PS-*b*-PMMA BCP was synthesized *via* RAFT polymerization. Meldrum's acid-based materials were used for thermal cross-linking as reported previously.[33,34] All chemicals were purchased from Sigma-Aldrich (St. Louis, MO, USA) and used as received except when mentioned specifically. The functional comonomer containing Meldrum's acid was synthesized using a one-step process from two commercially available materials, 2,2,5-trimethyl-1,3-dioxane-4,6-dione (5-methyl Meldrum's acid) and 4-vinylbenzyl chloride, under mild basic conditions; the crude product was recrystallized to afford the desired monomer as an analytically pure crystalline solid.[33,34] The resulting comonomer is denoted as Meldrum's acid monomer. For the polymerization, methyl methacrylate (50 g, 499 mmol), 2,20-azobis-(2-methylpropionitrile) (AIBN) (24 mg, 0.15 mmol), and RAFT agent (450 mg, 1.50 mmol) were mixed and degassed. The reaction was carried out at 70 °C for 12 h. The reaction product was then precipitated into cold methanol, resulting in a PMMA-RAFT macroinitiator as a pink powder (M_n = 19 000 g/mol and PDI = 1.10). To add the cross-linkable block, PMMA-RAFT (10 g), styrene (71.9 g), Meldrum's acid monomer (5.85 g), and AIBN (0.0082 g) were mixed and degassed. The reaction was carried out at 70 °C for 48 h. The reaction product was then precipitated into cold methanol, resulting in cross-linkable PS-*b*-PMMA BCP as a pink powder (M_n = 61 kg/mol, PDI = 1.09).

Fabrication of the HPS. To prepare various topographical patterns, a silicon wafer was first neutralized using the cross-linkable PS-*r*-PMMA random copolymer as reported previously.[34] The PS-*r*-PMMA solution in toluene [0.4% (w/w)] was spin-coated on a 6-in. silicon wafer (3000 rpm, 120 s). The films were thermally cross-linked under N_2 for 10 min. Thin films of cross-linkable PS-*b*-PMMA BCP were prepared on these substrates by spin-casting the toluene solutions. The thickness of the BCP films was controlled to be 35 nm. The films were then annealed at 190 °C for 48 h under a vacuum. To secure solvent resistance, the cylindrical layer was subsequently cross-linked at 250 °C for 10 min under inert N_2 (for nanopore patterns). The microgroove structures were prepared using an I-line photolithography process with a negative photoresist (SU-8) on top of the neutral layer (for microgroove patterns) or a cross-linked cylindrical layer (for hierarchical patterns). To remove the PMMA microdomain, the reactive ion etching (RIE system SNTEK, SNTEK, Suwon, Korea) mode was operated with Ar (3 sccm)/O_2 (15 sccm) by an RF power of 20 W at 0.1 Torr.

Substrate Characterization. Gel permeation chromatography (GPC) was performed in THF on a Waters instrument equipped with a refractive index detector (Waters 2414, Waters, Milford, MA, USA). Molecular weights of the polymers were calculated relative to linear polystyrene standards. Film morphologies were examined by field-emission scanning electron microscopy (FE-SEM, S-4800, Hitachi, Tokyo, Japan).

hNSC Culture. hNSCs were derived from the telencephalon (HFT13) as previously described.[49] hNSCs were cultured at a density of 6.0 × 10^5/ml in Dulbecco's Modified Eagle's Medium/Nutrient Mixture F-12 (DMEM/F12) medium (Gibco, Gaithersburg, MD, USA) supplemented with bFGF (20 ng/mL, Sigma), LIF (10 ng/mL, Sigma), and N-2 supplement (Gibco) in humidified air with 5% CO_2 at 37 °C. hNSCs were grown as neurospheres under these conditions. Single hNSCs dissociated from the neurospheres were seeded onto the substrates and cultured at a density of 3.5 × 10^5 cells/mL. To induce spontaneous differentiation, hNSCs were maintained in DMEM/F12 medium without supplementation of mitogenic factors (bFGF and LIF). The FS was used as a negative control. All substrates were coated with 10 μg/mL fibronectin (Sigma) to facilitate hNSC adhesion. After 5 days in culture, hNSC differentiation was analyzed by immunocytochemical staining and qRT-PCR.

Immunocytochemistry. Immunocytochemical staining of hNSCs was performed as previously described.[4] hNSCs cultured on the substrates were fixed with 4% (w/v) paraformaldehyde (Sigma) for 15 min and then permeabilized with 0.1% (v/v) Triton X-100 (Sigma) for 5 min. After blocking with 2% (v/v) goat serum (sigma) for 45 min, hNSCs were incubated with primary antibodies at 4 °C overnight. The following primary antibodies were

used for staining: mouse monoclonal anti-Tuj1 (1:100; Millipore, Temecula, CA, USA), rabbit polyclonal anti-MAP2 (1:200; Santa Cruz Biotechnology, Santa Cruz, CA, USA), mouse monoclonal anti-GFAP (1:200; Millipore), rabbit polyclonal antinestin (1:200; Abcam, Cambridge, UK), mouse monoclonal anti-O4 (1:100; Millipore), rabbit polyclonal anti-NCAM (1:200; Millipore), and mouse monoclonal anti-integrin β1 (1:200; Millipore). After washing with phosphate-buffered saline (PBS), secondary antibodies [Alexa Fluor-488 goat antimouse IgG (1:500) and Alexa Fluor-594 donkey antirabbit IgG (1:500); Invitrogen, Carlsbad, CA, USA] were added and incubated with the cells for 45 min. Cell nuclei were counterstained with 4′,6-diamidino-2-phenylindole (DAPI, Sigma). The fluorescently stained signals were observed under a confocal microscope (LSM 700, Carl Zeiss, Jena, Germany). Neurite formation was quantified as the percentage ratio of Tuj1-positive cells with neurites to total cells (DAPI-positive cells). The length of neurite outgrowth was quantified by measuring the length of the projections from Tuj1-positive cell body.

Focal Adhesion and Cytoskeleton Staining. The hNSCs on the substrates were stained for the cytoskeleton (F-actin), focal adhesion protein (vinculin), and nucleus using the Actin Cytoskeleton and Focal Adhesion Staining Kits (FAK100) (Millipore) according to the manufacturer's instructions. The stained signals were observed under a confocal microscope (LSM 700, Carl Zeiss). The proportion of nonadherent cells was defined as the percentage ratio of vinculin-negative cells to total cell population (DAPI-positive cells) in the vinculin- and F-actin-stained images of hNSCs.

qRT-PCR. Total RNA for qRT-PCR analysis was prepared using an RNeasy Mini kit (Qiagen, Chatsworth, CA, USA) for each sample (n = 3 per group) according to the manufacturer's instructions. RNA concentration was determined by measuring the absorbance of the samples at 260 nm using a spectrophotometer. Reverse transcription to prepare cDNA from each RNA sample was performed using a TaKaRa PrimeScript II First Strand cDNA Synthesis Kit (TaKaRa, Shiga, Japan). qRT-PCR was performed using a StepOnePlus Real-Time PCR System (Applied Biosystems, Foster City, CA, USA) as previously described.[49] TaqMan Fast Universal PCR Master Mix (Applied Biosystems) was used for the reaction. The gene expression profiles in hNSCs were quantified using TaqMan Gene Expression Assays (Applied Biosystems) for each target (Tuj1: Hs00801390_s1, MAP2: Hs00258900_m1, GFAP: Hs00909238_g1, FAK: Hs01056457_m1, vinculin: Hs00419715_m1, olig2: Hs00300164_s1, and nestin: Hs00707120_s1). The relative expression level of each target gene was determined using the comparative C_t method, where the expression was normalized to that of an endogenous reference transcript (human GAPDH: Hs02758991_g1).[50]

SEM. The hNSC morphology on the substrates was observed by SEM hNSCs on the substrates were fixed with 4% paraformaldehyde for 1 h and rinsed with PBS three times. The samples were dehydrated using a graded series of ethanol (50, 70, 80, 90, and 100% for 10 min each) and dried. The dried samples were mounted on an aluminum stub, sputter-coated with platinum, and imaged by SEM (FEI XL 30 ESEM, Philips, Eindhoven, Netherlands).

Western Blot. Total protein was extracted from hNSCs grown on each substrate using a RIPA lysis buffer (Sigma) and a protease inhibitor cocktail (Roche Diagnostics, Mannheim, Germany). The concentrations of total protein in each sample were determined using a BCA assay kit (Thermo Scientific, Waltham, MA, USA). The proteins in each sample were separated by 10% sodium dodecyl sulfate-polyacrylamide gel electrophoresis and transferred onto polyvinylidene fluoride membranes (Millipore). The membranes were blocked with 5% skim milk for 1 h at room temperature and incubated overnight with primary antibodies [rabbit polyclonal anti-FAK (pY397, 1:1000; Invitrogen), rabbit polyclonal anti-MAP2 (1:500; Santa Cruz Biotechnology), rabbit monoclonal anti-α-tubulin (1:2500; Cell Signaling, Beverly, MA, USA), and rabbit polyclonal anti-TBP (1:500; Cell Signaling)] at 4 °C. The signals of the target proteins were detected using a Clarity Western ECL Substrate (Bio-Rad, Hercules, CA, USA) according to the manufacturer's instructions.

Inhibition of Adhesion and Alignment of the Cytoskeleton. To inhibit cell adhesion onto fibronectin-coated substrates, the hNSCs were treated with anti-β1 integrin (1:40; Millipore). The cells were also treated with 10 μM Y27632 (Millipore) to inhibit the ROCK pathway involved in actin organization. One day after treatment, immunofluorescent staining for vinculin/F-actin and Tuj1/GFAP was performed. The stained signals were observed under a confocal microscope (LSM 700, Carl Zeiss). The expression of differentiation markers (Tuj1 and GFAP) and focal adhesion proteins (vinculin and FAK) in NSCs treated with anti-integrin β1 and Y27632 was quantified by qRT-PCR and normalized to the expression in hNSCs on the FS without treatment. The viability of hNSCs on each substrate 1 day after treatments of anti-β1 integrin and Y27632 was examined using a Live/Dead viability kit (Invitrogen, Carlsbad, CA, USA). In this assay, calcein AM stains the cytoplasm of viable cells green and ethidium homodimer stains the nuclei of nonviable cells red. The mitochondrial metabolic activity of hNSCs was determined by MTT assay (Sigma) 1 day after treatments. The mitochondrial metabolic activity of hNSCs on each substrate was normalized to that of nontreated hNSCs on the FS.

Examination of Neuronal Phenotype of hNSCs Harvested from the HPS. The hNSCs cultured on each substrate for 5 days were detached from the substrates and transferred onto flat polystyrene tissue culture plate at a density 3.0×10^5 cells/ml. The hNSCs were maintained in DMEM/F12 medium without supplementation of bFGF and LIF. Neuronal phenotype of the hNSCs was examined by microscopic observation and immunocytochemical staining for a neuronal marker (Tuj1) after 4 days in culture.

Electrophysiology. For electrophysiological recording of differentiated hNSCs on the HPS, the coverslip with cultured cells on was transferred to the recording chamber (Warner Instrument, Hamden, CT, USA) and placed on the microscope (Olympus, Japan) while continuously superfusing with artificial cerebrospinal fluid (aCSF) containing 124 mM NaCl, 3 mM KCl, 1.3 mM $MgSO_4$, 1.25 mM NaH_2PO_4, 26 mM $NaHCO_3$, 2.4 mM $CaCl_2$-$2H_2O$, and 10 mM glucose. The solution was continuously aerated by O_2 95%/CO_2 5% mixed gas at room temperature. Whole cell patch clamping was performed by glass capillary pipet tips that were fabricated by pipet puller (P-97, Sutter Instrument, Novato, CA, USA) and filled with internal pipet solution. Glass capillary pipet was carefully located onto the cell surface and negative pressure was carefully applied to form gigaseal between glass pipet and cell membrane. Attached cell membrane was ruptured to generate whole cell configuration. Internal pipet solution contains 115 mM K-gluconate, 10 mM KCl, 10 mM HEPES, 10 mM EGTA, 5 mM Mg-ATP, and 0.5 mM Na^{2+}-GTP, with pH 7.3 and 280−285 mOsm. Holding potential was −60 mV and voltage steps ranging from −60 to +50 mV (+10 mV per each step) were given to the cell to elicit the voltage activated currents in voltage clap mode. In current clamp mode to check the generation of action potential, the cells received 15 steps of current steps (initial level = 0 pA, Δ10−20 pA per steps). Δ value was adjusted according to the membrane capacity of the cells. To identify that currents and spikes are specific to Na^+ channel, 0.5 μM TTX (Sigma-Aldrich) was applied into the bath for 5−10 min.

Statistical Analysis. Quantitative data are expressed as the mean ± standard deviation. Statistical analyses were performed using a one-way analysis of variance (ANOVA) followed by Tukey's multiple comparison test (SPSS Statistics 21.0, IBM SPSS, Armonk, NY, USA) as previously described.[51] Values of p less than 0.01 or 0.05 were considered statistically significant.

Conflict of Interest: The authors declare no competing financial interest.

Acknowledgment. This work was supported by grants (NRF-2010-0020409, NRF-2013R1A1A2A10061422, NRF-2012R1A2-A2A01014473, NRF-2012M3A7B4049863, and NRF-2013022350) from the National Research Foundation of Korea (NRF) and a grant (2009-0083522) from the Translational Research Center for Protein Function Control (TRCP) funded by the Ministry of Science, ICT, and Future Planning (MSIP), Republic of Korea. This work was also supported by the Advanced Biomass R&D Center (ABC) for the Global Frontier Project (ABC-2011-0031356) funded by the MSIP.

Supporting Information Available: Supplementary figures. This material is available free of charge *via* the Internet at http://pubs.acs.org.

REFERENCES AND NOTES

1. Schuldiner, M.; Eiges, R.; Eden, A.; Yanuka, O.; Itskovitz-Eldor, J.; Goldstein, R. S.; Benvenisty, N. Induced Neuronal Differentiation of Human Embryonic Stem Cells. *Brain Res.* **2001**, *913*, 201–205.
2. Blurton-Jones, M.; Kitazawa, M.; Martinez-Coria, H.; Castello, N. A.; Müller, F.-J.; Loring, J. F.; Yamasaki, T. R.; Poon, W. W.; Green, K. N.; LaFerla, F. M. Neural Stem Cells Improve Cognition *via* BDNF in a Transgenic Model of Alzheimer Disease. *Proc. Natl. Acad. Sci. U. S. A.* **2009**, *106*, 13594–13599.
3. Discher, D. E.; Mooney, D. J.; Zandstra, P. W. Growth Factors, Matrices, and Forces Combine and Control Stem Cells. *Science* **2009**, *324*, 1673–1677.
4. Yang, K.; Lee, J. S.; Kim, J.; Lee, Y. B.; Shin, H.; Um, S. H.; Kim, J. B.; Park, K. I.; Lee, H.; Cho, S. W. Polydopamine-Mediated Surface Modification of Scaffold Materials for Human Neural Stem Cell Engineering. *Biomaterials* **2012**, *33*, 6952–6964.
5. Ko, E.; Yang, K.; Shin, J.; Cho, S. W. Polydopamine-Assisted Osteoinductive Peptide Immobilization of Polymer Scaffolds for Enhanced Bone Regeneration by Human Adipose-Derived Stem Cells. *Biomacromolecules* **2013**, *14*, 3202–3213.
6. Engler, A. J.; Sen, S.; Sweeney, H. L.; Discher, D. E. Matrix Elasticity Directs Stem Cell Lineage Specification. *Cell* **2006**, *126*, 677–689.
7. Cameron, A. R.; Frith, J. E.; Cooper-White, J. J. The Influence of Substrate Creep on Mesenchymal Stem Cell Behaviour and Phenotype. *Biomaterials* **2011**, *32*, 5979–5993.
8. Trappmann, B.; Gautrot, J. E.; Connelly, J. T.; Strange, D. G.; Li, Y.; Oyen, M. L.; Stuart, M. A. C.; Boehm, H.; Li, B.; Vogel, V. Extracellular-Matrix Tethering Regulates Stem-Cell Fate. *Nat. Mater.* **2012**, *11*, 642–649.
9. Yamamoto, K.; Takahashi, T.; Asahara, T.; Ohura, N.; Sokabe, T.; Kamiya, A.; Ando, J. Proliferation, Differentiation, and Tube Formation by Endothelial Progenitor Cells in Response to Shear Stress. *J. Appl. Phys.* **2003**, *95*, 2081–2088.
10. Swift, J.; Ivanovska, I. L.; Buxboim, A.; Harada, T.; Dingal, P. C.; Pinter, J.; Pajerowski, J. D.; Spinler, K. R.; Shin, J. W.; Tewari, M.; *et al.* Nuclear Lamin-a Scales with Tissue Stiffness and Enhances Matrix-Directed Differentiation. *Science* **2013**, *341*, 1240104.
11. Dalby, M. J.; Gadegaard, N.; Tare, R.; Andar, A.; Riehle, M. O.; Herzyk, P.; Wilkinson, C. D.; Oreffo, R. O. The Control of Human Mesenchymal Cell Differentiation Using Nanoscale Symmetry and Disorder. *Nat. Mater.* **2007**, *6*, 997–1003.
12. Yao, X.; Peng, R.; Ding, J. Effects of Aspect Ratios of Stem Cells on Lineage Commitments with and without Induction Media. *Biomaterials* **2013**, *34*, 930–939.
13. Aizawa, Y.; Shoichet, M. S. The Role of Endothelial Cells in the Retinal Stem and Progenitor Cell Niche within a 3d Engineered Hydrogel Matrix. *Biomaterials* **2012**, *33*, 5198–5205.
14. Guerrero, J.; Catros, S.; Derkaoui, S. M.; Lalande, C.; Siadous, R.; Bareille, R.; Thebaud, N.; Bordenave, L.; Chassande, O.; Le Visage, C.; *et al.* Cell Interactions between Human Progenitor-Derived Endothelial Cells and Human Mesenchymal Stem Cells in a Three-Dimensional Macroporous Polysaccharide-Based Scaffold Promote Osteogenesis. *Acta Biomater.* **2013**, *9*, 8200–8213.
15. Guvendiren, M.; Burdick, J. A. Stem Cell Response to Spatially and Temporally Displayed and Reversible Surface Topography. *Adv. Healthcare Mater.* **2013**, *2*, 155–164.
16. Yim, E. K.; Darling, E. M.; Kulangara, K.; Guilak, F.; Leong, K. W. Nanotopography-Induced Changes in Focal Adhesions, Cytoskeletal Organization, and Mechanical Properties of Human Mesenchymal Stem Cells. *Biomaterials* **2010**, *31*, 1299–1306.
17. Teo, B. K.; Wong, S. T.; Lim, C. K.; Kung, T. Y.; Yap, C. H.; Ramagopal, Y.; Romer, L. H.; Yim, E. K. Nanotopography Modulates Mechanotransduction of Stem Cells and Induces Differentiation through Focal Adhesion Kinase. *ACS Nano* **2013**, *7*, 4785–4798.
18. Teo, B. K.; Ankam, S.; Chan, L. Y.; Yim, E. K. Nanotopography/Mechanical Induction of Stem-Cell Differentiation. *Methods Cell Biol.* **2010**, *98*, 241–294.
19. Lee, M. R.; Kwon, K. W.; Jung, H.; Kim, H. N.; Suh, K. Y.; Kim, K.; Kim, K.-S. Direct Differentiation of Human Embryonic Stem Cells into Selective Neurons on Nanoscale Ridge/Groove Pattern Arrays. *Biomaterials* **2010**, *31*, 4360–4366.
20. Ahn, E. H.; Kim, Y.; Kshitiz, A. S. S.; Afzal, J.; Lee, S.; Kwak, M.; Suh, K. Y.; Kim, D. H.; Levchenko, A. Spatial Control of Adult Stem Cell Fate Using Nanotopographic Cues. *Biomaterials* **2014**, *35*, 2401–2410.
21. Ankam, S.; Suryana, M.; Chan, L. Y.; Moe, A. A.; Teo, B. K.; Law, J. B.; Sheetz, M. P.; Low, H. Y.; Yim, E. K. Substrate Topography and Size Determine the Fate of Human Embryonic Stem Cells to Neuronal or Glial Lineage. *Acta Biomater.* **2013**, *9*, 4535–4545.
22. Yang, K.; Jung, K.; Ko, E.; Kim, J.; Park, K. I.; Kim, J.; Cho, S.-W. Nanotopographical Manipulation of Focal Adhesion Formation for Enhanced Differentiation of Human Neural Stem Cells. *ACS Appl. Mater. Interfaces* **2013**, *5*, 10529–10540.
23. Kim, M. J.; Lee, B.; Yang, K.; Park, J.; Jeon, S.; Um, S. H.; Kim, D. I.; Im, S. G.; Cho, S. W. BMP-2 Peptide-Functionalized Nanopatterned Substrates for Enhanced Osteogenic Differentiation of Human Mesenchymal Stem Cells. *Biomaterials* **2013**, *34*, 7236–7246.
24. Tay, C. Y.; Yu, H.; Pal, M.; Leong, W. S.; Tan, N. S.; Ng, K. W.; Leong, D. T.; Tan, L. P. Micropatterned Matrix Directs Differentiation of Human Mesenchymal Stem Cells Towards Myocardial Lineage. *Exp. Cell. Res.* **2010**, *316*, 1159–1168.
25. Xiong, J. P.; Stehle, T.; Zhang, R.; Joachimiak, A.; Frech, M.; Goodman, S. L.; Arnaout, M. A. Crystal Structure of the Extracellular Segment of Integrin Alpha Vbeta3 in Complex with an Arg-Gly-Asp Ligand. *Science* **2002**, *296*, 151–155.
26. Wang, X.; Yan, C.; Ye, K.; He, Y.; Li, Z.; Ding, J. Effect of RGD Nanospacing on Differentiation of Stem Cells. *Biomaterials* **2013**, *34*, 2865–2874.
27. Petrie, T. A.; Raynor, J. E.; Dumbauld, D. W.; Lee, T. T.; Jagtap, S.; Templeman, K. L.; Collard, D. M.; Garcia, A. J. Multivalent Integrin-Specific Ligands Enhance Tissue Healing and Biomaterial Integration. *Sci. Transl. Med.* **2010**, *2*, 45ra60.
28. Moe, A. A.; Suryana, M.; Marcy, G.; Lim, S. K.; Ankam, S.; Goh, J. Z.; Jin, J.; Teo, B. K.; Law, J. B.; Low, H. Y.; *et al.* Microarray with Micro- and Nano-Topographies Enables Identification of the Optimal Topography for Directing the Differentiation of Primary Murine Neural Progenitor Cells. *Small* **2012**, *8*, 3050–3061.
29. Bang, J.; Jeong, U.; Ryu, D. Y.; Russell, T. P.; Hawker, C. J. Block Copolymer Nanolithography: Translation of Molecular Level Control to Nanoscale Patterns. *Adv. Mater.* **2009**, *21*, 4769–4792.
30. Stoykovich, M. P.; Nealey, P. F. Block Copolymers and Conventional Lithography. *Mater. Today* **2006**, *9*, 20–29.
31. Hawker, C. J.; Russell, T. P. Block Copolymer Lithography: Merging "Bottom-up" with "Top-Down" Processes. *MRS Bull.* **2005**, *30*, 952–966.
32. Bang, J.; Bae, J.; Löwenhielm, P.; Spiessberger, C.; Given-Beck, S. A.; Russell, T. P.; Hawker, C. J. Facile Routes to Patterned Surface Neutralization Layers for Block Copolymer Lithography. *Adv. Mater.* **2007**, *19*, 4552–4557.
33. Leibfarth, F. A.; Kang, M.; Ham, M.; Kim, J.; Campos, L. M.; Gupta, N.; Moon, B.; Hawker, C. J. A Facile Route to Ketene-Functionalized Polymers for General Materials Applications. *Nat. Chem.* **2010**, *2*, 207–212.
34. Jung, H.; Leibfarth, F. A.; Woo, S.; Lee, S.; Kang, M.; Moon, B.; Hawker, C. J.; Bang, J. Efficient Surface Neutralization and Enhanced Substrate Adhesion through Ketene Mediated Crosslinking and Functionalization. *Adv. Funct. Mater.* **2012**, *23*, 1597–1602.

35. Jung, H.; Hwang, D.; Kim, E.; Kim, B.-J.; Lee, W. B.; Poelma, J. E.; Kim, J.; Hawker, C. J.; Huh, J.; Ryu, D. Y. Three-Dimensional Multilayered Nanostructures with Controlled Orientation of Microdomains from Cross-Linkable Block Copolymers. *ACS Nano* **2011**, *5*, 6164–6173.
36. Chen, Y.-C.; Lee, D.-C.; Tsai, T.-Y.; Hsiao, C.-Y.; Liu, J.-W.; Kao, C.-Y.; Lin, H.-K.; Chen, H.-C.; Palathinkal, T. J.; Pong, W.-F. Induction and Regulation of Differentiation in Neural Stem Cells on Ultra-Nanocrystalline Diamond Films. *Biomaterials* **2010**, *31*, 5575–5587.
37. Wang, X.; Song, W.; Kawazoe, N.; Chen, G. The Osteogenic Differentiation of Mesenchymal Stem Cells by Controlled Cell-Cell Interaction on Micropatterned Surfaces. *J. Biomed. Mater. Res., Part A* **2013**, *101*, 3388–3395.
38. Hynes, R. O. Integrins: Versatility, Modulation, and Signaling in Cell Adhesion. *Cell* **1992**, *69*, 11–25.
39. Kuo, S. W.; Lin, H. I.; Ho, J. H.; Shih, Y. R.; Chen, H. F.; Yen, T. J.; Lee, O. K. Regulation of the Fate of Human Mesenchymal Stem Cells by Mechanical and Stereo-Topographical Cues Provided by Silicon Nanowires. *Biomaterials* **2012**, *33*, 5013–5022.
40. Seo, C. H.; Furukawa, K.; Montagne, K.; Jeong, H.; Ushida, T. The Effect of Substrate Microtopography on Focal Adhesion Maturation and Actin Organization *via* the Rhoa/Rock Pathway. *Biomaterials* **2011**, *32*, 9568–9575.
41. Seo, C. H.; Jeong, H.; Feng, Y.; Montagne, K.; Ushida, T.; Suzuki, Y.; Furukawa, K. S. Micropit Surfaces Designed for Accelerating Osteogenic Differentiation of Murine Mesenchymal Stem Cells *via* Enhancing Focal Adhesion and Actin Polymerization. *Biomaterials* **2014**, *35*, 2245–2252.
42. Shih, Y. R.; Tseng, K. F.; Lai, H. Y.; Lin, C. H.; Lee, O. K. Matrix Stiffness Regulation of Integrin-Mediated Mechanotransduction During Osteogenic Differentiation of Human Mesenchymal Stem Cells. *J. Bone Miner. Res.* **2011**, *26*, 730–738.
43. Sun, Y.; Yong, K. M.; Villa-Diaz, L. G.; Zhang, X.; Chen, W.; Philson, R.; Weng, S.; Xu, H.; Krebsbach, P. H.; Fu, J. Hippo/Yap-Mediated Rigidity-Dependent Motor Neuron Differentiation of Human Pluripotent Stem Cells. *Nat. Mater.* **2014**, *13*, 599–604.
44. Yang, C.; Tibbitt, M. W.; Basta, L.; Anseth, K. S. Mechanical Memory and Dosing Influence Stem Cell Fate. *Nat. Mater.* **2014**, *13*, 645–652.
45. Dupont, S.; Morsut, L.; Aragona, M.; Enzo, E.; Giulitti, S.; Cordenonsi, M.; Zanconato, F.; Le Digabel, J.; Forcato, M.; Bicciato, S.; *et al.* Role of Yap/Taz in Mechanotransduction. *Nature* **2011**, *474*, 179–183.
46. Zala, D.; Hinckelmann, M. V.; Yu, H.; Lyra da Cunha, M. M.; Liot, G.; Cordelieres, F. P.; Marco, S.; Saudou, F. Vesicular Glycolysis Provides on-Board Energy for Fast Axonal Transport. *Cell* **2013**, *152*, 479–491.
47. Morgan, P. J.; Liedmann, A.; Hubner, R.; Hovakimyan, M.; Rolfs, A.; Frech, M. J. Human Neural Progenitor Cells Show Functional Neuronal Differentiation and Regional Preference after Engraftment onto Hippocampal Slice Cultures. *Stem Cells Dev.* **2012**, *21*, 1501–1512.
48. Vukicevic, V.; Schmid, J.; Hermann, A.; Lange, S.; Qin, N.; Gebauer, L.; Chunk, K. F.; Ravens, U.; Eisenhofer, G.; Storch, A.; *et al.* Differentiation of Chromaffin Progenitor Cells to Dopaminergic Neurons. *Cell Transplant.* **2012**, *21*, 2471–2486.
49. Yang, K.; Han, S.; Shin, Y.; Ko, E.; Kim, J.; Park, K. I.; Chung, S.; Cho, S.-W. A Microfluidic Array for Quantitative Analysis of Human Neural Stem Cell Self-Renewal and Differentiation in Three-Dimensional Hypoxic Microenvironment. *Biomaterials* **2013**, *34*, 6607–6614.
50. Cho, S. W.; Goldberg, M.; Son, S. M.; Xu, Q.; Yang, F.; Mei, Y.; Bogatyrev, S.; Langer, R.; Anderson, D. G. Lipid-Like Nanoparticles for Small Interfering RNA Delivery to Endothelial Cells. *Adv. Funct. Mater.* **2009**, *19*, 3112–3118.
51. Savic, R.; Azzam, T.; Eisenberg, A.; Maysinger, D. Assessment of the Integrity of Poly(Caprolactone)-*b*-Poly(Ethylene Oxide) Micelles under Biological Conditions: A Fluorogenic-Based Approach. *Langmuir* **2006**, *22*, 3570–3578.